HAL
open science

Modeling the Hydrolysis of Iron–Sulfur Clusters

Murilo H. Teixeira, Felipe Curtolo, Sofia R. G. Camilo, Martin J. Field, Peng Zheng, Hongbin Li, Guilherme M. Arantes

▶ To cite this version:

HAL Id: hal-02494443
https://hal.science/hal-02494443

Submitted on 24 Oct 2022

Modelling the hydrolysis of iron-sulfur clusters

Murilo H. Teixeira, Felipe Curtolo, Sofia R. G. Camilo, Martin J. Field, Peng Zheng, Hongbin Li and Guilherme M. Arantes[*]

Department of Biochemistry, Instituto de Química, Universidade de São Paulo, Av. Prof. Lineu Prestes 748, 05508-900, São Paulo, SP, Brazil

E-mail: garantes@iq.usp.br

Abstract

Iron-sulfur (FeS) clusters are essential metal cofactors involved in a wide variety of biological functions. Their stability, biosynthesis and catalytic mechanisms depend on FeS reactivity in aqueous solution. Here, molecular modelling is used to investigate the hydrolysis of an oxidized (ferric) mononuclear FeS cluster by bare dissociation and substitution mechanisms in neutral and acidic solution. First, an approximate electronic structure descriptions of FeS reactions by density functional theory are validated against high-level wave-function CCSD(T) calculations. Solvation contributions are evaluated by an all-atom model with hybrid quantum chemical/molecular mechanical (QM/MM) potential and enhanced sampling molecular dynamics simulations. The free energy profile obtained for FeS cluster hydrolysis indicates the hybrid functional M06 added with an implicit solvent correction may capture the most important aspects of FeS cluster reactivity in aqueous solution. Then, up to 20 reaction channels leading to two consecutive Fe–S bond ruptures were explored with this calibrated model. Nucleophilic substitution with concerted bond breaking and forming to iron is the preferred mechanism, both kinetic and thermodynamically, for all protonation states. In neutral solution, proton transfer from water to the sulfur leaving group is also observed simultaneously. Dissociative reactions show higher barriers and will not be relevant for FeS reactivity when exposed to solvent. The hydrolysis mechanisms presented here may help to explain the stability and catalytic mechanisms of FeS clusters of multiple sizes and protein partners.

---

[*]To whom correspondence should be addressed

1 Introduction

Iron and sulfur are abundant elements on the Earth surface. They were recruited in the form of iron-sulfur (FeS) clusters early during the evolution of life resulting in ancient proteins with the ability to catalyze electron transfer reactions.[1] Essential biological processes such as cellular respiration and photosynthesis rely on enzymes equipped with FeS clusters. In fact, the largest class of metalloproteins comprise proteins which carry FeS clusters as cofactors.[2] From structural and electronic points of view, FeS clusters sit between transition metal atoms and solid surfaces.[3] Usually, they are formed by 1, 2, 4 or 8 iron nuclei (mostly in ferric form but turn to ferrous when reduced) bridged by inorganic sulfide anions and connected to the protein scaffold by thiolate groups in cystein side-chains.

The stability and biosynthesis of FeS clusters will naturally depend on their reactivity in aqueous solution. Catalytic mechanisms and regulation of enzymes enclosing FeS clusters are also modulated by the connectivity of Fe–S bonds. In nitrogenase, sulfide hemilability has been observed as an intermediate step for CO/H_2 exchange in the reduction cycle of the FeMo cofactor.[4,5] In aconitase, the FeS cluster directly coordinates the citrate substrate and may break down in response to cellular levels of iron.[6]

The reactivity of protein-bound FeS clusters with molecular oxygen has been studied experimentally in detail, since an oxidative environment may convert exposed FeS clus-

ters to unstable species that quickly decompose.[5,7] But, their stability upon hydrolysis and substitution reactions has received less attention, partially because FeS clusters are often buried in proteins. Synthetic FeS analogues have been studied extensively and provided details of ligand exchange and protonation chemistry.[7,8] Another elegant approach based on single-molecule force spectroscopy has been proposed recently to partially unfold and expose FeS clusters, allowing to study their reactivity in biologically relevant conditions.[9–12]

Quantum chemical calculations including environmental effects may also be used to investigate the reactivity of transition metal complexes in solution.[13] But modelling FeS clusters is particularly challenging. Besides the multiple Fe–S bonds, several protonation, oxidation and spin states may be populated, resulting in an explosion of possible reactive channels.[3] Their electronic structure show many low-lying and near-degenerate states that may cross, leading to multiple-state reactivity.[14,15] In polynuclear FeS clusters, strong electron correlation and long-range spin coupling effects complicate enormously the theoretical description[16,17] such that electronic structure calculations on FeS clusters have been proposed as an example where upcoming quantum computers could exceed the power of classical supercomputers.[18]

Here, we look into the stability of FeS clusters starting with a rather pedestrian model, a mononuclear iron center bound to four thiolate ligands, [1Fe-4S]. This is the simplest FeS cluster and reflects the cofactor found in rubredoxin, a protein in gram-negative bacteria.[19] Appling several electronic structure methods, we investigate exhaustively the reactions of the model compound $Fe(SCH_3)_4^-$ with water or bare dissociation in various protonation states and mechanisms up to the second Fe–S bond rupture, as described in Fig. 1.

The remainder of the text is organized as follows. Given the intricate electronic structure of FeS clusters, we initially benchmark the performance of approximate density functional theory (DFT) against high-level quantum chemical (QC) calculations. Free energy
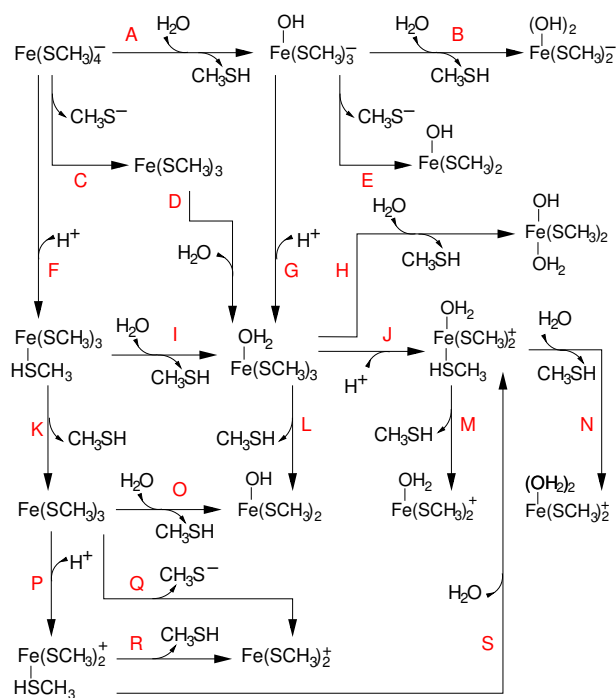

Figure 1: Scheme of the iron-sulfur reactions studied here. Substitution reactions (AnDn in the current nomenclature[20]) are denoted with water input and leaving group output concomitant arrows. Dissociation reactions (Dn) show only the output leaving group arrow. Reaction S is the only addition reaction (An) shown. Molecules $Fe(SCH_3)_3$ (formed by reactions C and K) and $Fe(OH)(SCH_3)2$ (formed by reactions E, L and O) are repeated to avoid a clumsy scheme.

contributions and solvation effects captured by explicit all-atom hybrid QM/MM simulations are compared to models using implicit solvation to find an efficient yet reliable DFT description of FeS stability in aqueous solution. Readers only interested in FeS reactivity can skip all methodological details and model calibration, and jump to section 3.3 where FeS hydrolysis reactions are discussed.

2 Methods

2.1 Quantum chemical calculations

All molecular geometries for stationary points (reactants, products and transition states, TS) were optimized with the OLYP[21,22] functional, the 6-31+G(2df,p)[23] basis set and the PCM implicit water solvation model[24] with the Gaussian 09 program (Rev. A1).[25] Pre-

vious calculations showed this functional provides a reasonable description of Fe–S bond dissociation.[26] Two-dimensional scans were used to search for TS in substitution (AnDn) reactions, restraining both forming (Fe–O) and breaking (Fe–S) bonds in a linear combination as well as the proton coordinate when this atom was transferred to the sulfur leaving group (see more details of reaction coordinates below). These scans were done with the pDynamo library[27] version 1.9 interfaced with ORCA program version 3.0.1,[28] the OLYP functional, the def2-SVP basis set[29] and the COSMO implicit water model.[30] Iron compounds were always in the oxidized and spin sextet states.

Zero-point energies, thermal and entropic contributions were evaluated for stationary points using vibrational frequencies and the harmonic oscillator and rigid rotor approximations.[31] No empirical scaling was applied to frequencies.[32]

Single-point energies for isolated optimized geometries were obtained with the ORCA program version 3.0.1[28] and the following functionals: OLYP, OPBE,[21,33] B3LYP,[22,34] TPSS,[35] M06,[36] M06L,[37] B97 and ωB97X.[38] Spin-polarized orbitals and standard integration grids were adopted. The def2-TZVP basis set[29] and resolution of identity with the TZV/J[39] auxiliary basis were used. A second-order SCF optimization had to be activated to obtain convergence in several cases. All calculations were carried out in the C_1 point-group symmetry. Dispersion interactions were added to some DFT functionals with Grimme's D3 correction[40] using the Becke and Johnson' damping.[41,42] Relativistic effects were evaluated at the M06/def2-TZVP level with the Douglas-Kroll-Hess (DKH) approximation.

A semiempirical potential specifically parametrized to model Fe–S bond dissociation[26] based on the PM6 general parametrization[43] with d-orbitals was also tested. Complete active space configuration interaction (CASCI) calculations[44] with 7 electrons in 7 MOs space were performed with orbitals determined from restricted-open shell (ROHF) calculations with fractional occupation.[45,46] Semiempirical calculations were done with

the pDynamo library.[26]

Wave-function CCSD(T)[44] calculations with the domain based local pair natural orbital (DLPNO) approximation,[47] ROHF orbitals and the auxiliary basis def2-TZVP/C were obtained with ORCA version 4.1.1[48] and employed as reference energies for calibrations of the DFT methods.

2.2 Hybrid QM/MM free energy simulations in explicit solvent

Reaction A (Fig. 1) was simulated in explicit water with an all-atom model containing $Fe(SCH_3)_4^-$, 1689 water molecules and a Na^+ ion to neutralize the system, in a cubic box of 3.72 nm side. The system was initially relaxed during 2 ns of molecular dynamics simulation with a classical molecular mechanical (MM) potential and periodic boundary conditions using previous parameters for the FeS center,[15] CHARMM36[49] for Na^+, and TIP3P for water.[50] Then, all water molecules further than 16 Å from the Fe center were frozen and the remainder of the system relaxed again for 5 ps of molecular dynamics with a QM/MM potential, where only $Fe(SCH_3)_4^-$ and a harmonically restrained nearby water molecule were treat in the QC region with the OLYP/def2-SVP level of theory and all other atoms were treated in the MM region. A standard electrostatic QM/MM embedding without cut-offs or long-range electrostatic corrections was used as implemented in the pDynamo library 1.9 interfaced with ORCA 3.0.1.[27,51,52]

This system and QM/MM potential were used for umbrella sampling (US)[53] with molecular dynamics simulations of a two-dimension free energy profile for reaction A. Two reaction coordinates were employed: the difference between the distances of breaking (Fe–S) and forming (Fe–O) iron bonds, d(FeS)-d(FeO), described the iron reaction and the distance between a proton initially bound to water and the sulfur of the leaving group, d(SH), described the coupled proton transfer.[51,52] Reaction coordinates were explored between ranges -2.5 ≤ d(FeS)-d(FeO) ≤ 2.9 Å and 1.3 ≤ d(SH) ≤ 2.5 Å, separated by steps of 0.2Å and 0.3 Å, restrained

with harmonic potentials with force constant $k_{umb} = 1000$ and 500 kJ mol^{-1} Å^{-2}, respectively for the iron and the proton coordinates. A total of 146 US windows were sampled during 6 ps each, resulting in an aggregate simulation time with the QM(DFT)/MM potential of 0.9 ns. A Langevin dynamics integrator was used with a time-step of 1 fs, friction coefficient $\gamma = 25$ ps^{-1} and temperature of 300K.[54] The two-dimensional free energy surface was pieced together using the weighted histogram analysis method (WHAM)[55] with the initial 1 ps of each US window discarded for equilibration. Statistical uncertainties were estimated as 95% confidence intervals by bootstrap analysis.[56]

3   Results & Discussion

3.1   Performance of approximate electronic structure methods

Structures of transition-metal complexes determined with DFT methods are generally in good agreement with experiment.[57] However, iron-sulfur clusters show strong correlation effects that may not be described correctly by standard functionals. Previously, it was shown that left-right correlation important for the dissociation of Fe–S bonds is appropriately included in the OLYP functional,[26] so this method was employed here for geometry optimization and sampling. The quality of obtained structures may be accessed by the calculated Fe–S bond length for Fe(SCH$_3$)$_4^-$ (2.32 Å) which agrees reasonably with the Fe–S lengths (2.27-2.30 Å) observed in the high-resolution crystal structure of the [1Fe-4S] containing rubredoxin protein (PDB ID 8RXN).[19]

Table 1 shows the performance of several DFT functionals for calculating relative reaction energies and barriers in comparison to the gold-standard electronic structure method CCSD(T)[44] for 34 stationary points (products and TS) of all reactions in Fig. 1. No solvent contribution was included at this comparison. The lowest mean error is observed for the ωB97X-D3 range-separated hybrid functional with dispersion

Table 1: Performance of DFT and semiempirical methods in comparison to the CCSD(T) reference. Mean unsigned error (MUE) and maximum absolute error (MAE) are shown for relative energies (in kJ/mol) of 34 TS and product species in FeS cluster reactions shown in Fig. 1. All DFT calculations were done with the def2-TZVP basis set, except M06L/SVP and OLYP/SVP done with def2-SVP.

Functional	MUE	MAE
B3LYP	19.5	60.8
B3LYP-D3	9.2	28.9
B97-D3	13.9	31.8
M06	6.8	16.9
M06L	8.2	29.4
M06L/SVP	13.7	45.3
OLYP	27.4	81.5
OLYP/SVP	19.7	63.2
OPBE	24.9	69.0
PM6R	176.6	481.4
TPSS	13.7	52.7
ωB97X-D3	4.3	26.9

corrections, followed by the hybrid M06 functional, which shows the lowest maximum error. The MAE observed for all functionals tested correspond to the TS of reactions C and E where left-right (multi-configurational) correlation is significant.[26] The performance of B3LYP-D3 and M06L is also good. Comparison with B3LYP shows that addition of dispersion corrections is important and justifies the high performance of M06 and M06L which account for dispersion in the original parametrizations.[36] Fortuitous error-cancelation when using OLYP with smaller split-valence basis sets suggests that employing this level of theory should give reasonable results for geometry optimizations and sampling. Using a split-valence basis with M06L does not lead to such error-cancelation and degrades this functional performance.

Possible exceptions where dispersion effects may be essential for a correct structural description are TS for addition (An) and dissociation (Dn) steps involving neutral attacking or leaving groups, such as TS for reac-

tions D, K, L, M, R and S (Fig. 1). These species were re-optimized with the M06/6-31+G(2df,p) level of theory. Energy differences between re-optimized structures and the original OLYP geometries are smaller than 5 kJ/mol for TS_R and TS_S, around 10 kJ/mol for TS_D, TS_K and TS_M and 30 kJ/mol for TS_L. The considerable difference for the later species is due to an incomplete optimization done with OLYP and the floppy nature of this TS. These corrections were implemented in the results presented in section 3.3 but do not change any of the qualitative conclusions. Thus, even for FeS species where dispersion plays a major role, geometries obtained with the more approximate functional OLYP prove reasonable. Dispersion effects on geometries will be significantly smaller for reactant and product species, as well as for TS of the substitution (AnDn) reactions where stronger contributions such as electrostatic effects from H^+ transfer dominate.

The PM6R semiempirical method specifically calibrated for Fe–S dissociation reactions and 3 orders of magnitude faster than DFT methods was also tested.[26] Unfortunately, the method has unacceptable performance (Table 1) for all substitution reactions that involve oxygen atoms because this element was not included in the PM6R re-parametrization. Relativistic corrections within the DHK framework were also tested but their maximum contribution for relative energies relevant for FeS reactivity is only 3 kJ/mol, with an average of 1 kJ/mol. Thus, relativistic corrections were ignored in the remainder of this study.

Previously, the bare dissociation of Fe–S bonds was suggest to proceed through crossings between different spin states (quartets).[15] However, for substitution reactions with water and leaving group protonation (CH_3SH) studied here the energy gap between sextet and quartet states is more than 50 kJ/mol.[11]

An analysis of computational timings (Table S1) is necessary to find the best relation between accuracy and computational cost. The efficiency of DLPNO-CCSD(T) method is impressive and comparable to much more approximate hybrid and range-separated functionals. However, it is still impossible to run geometry optimizations with the DLPNO approximation since analytic gradients are not implemented and sampling millions of geometries necessary for free energy simulations would be prohibitively expensive. The hybrid functionals ωB97X-D3 and M06 give the best performance and may be applied for geometry optimizations but are still too expensive for sampling. The efficiency of M06L and other generalized gradient approximated (GGA) functionals is one order of magnitude better than the high performance hybrid functionals, but still too demanding for sampling. Acceptable efficiency is obtained with a split-valence basis set, so the OLYP/def2-SVP level was used as a reasonable compromise between accuracy and cost-effective DFT treatment for the hybrid potential free-energy simulations.

3.2 Free energies and solvation effects

The effect of water solvation on FeS reactivity was examined here for reaction A using two solvent models. This reaction was chosen as representative because it involves charged species and is important for FeS stability in aqueous solution (see section 3.3). We applied an all-atom explicit solvent model with a QM/MM hybrid potential description,[51,52,58] where individual water molecules may interact through electrostatic and van der Waals forces directly with the reactive molecules and polarize their electronic structure (see Fig. 2B for a model snapshot). This was compared with a more approximate implicit solvent model[24,59] where the electron cloud from reactive molecules are polarized by the dielectric response of a continuum that do not describe water structure or specific contacts (such as hydrogen bonds).

Reaction A actually involves two processes: iron transfer, *i.e.* breaking one Fe–S bond and forming the Fe–O bond with water, and proton transfer from water to the leaving group sulfur atom. These were described by distance reaction coordinates d(FeS)-d(FeO) and d(SH), respectively.
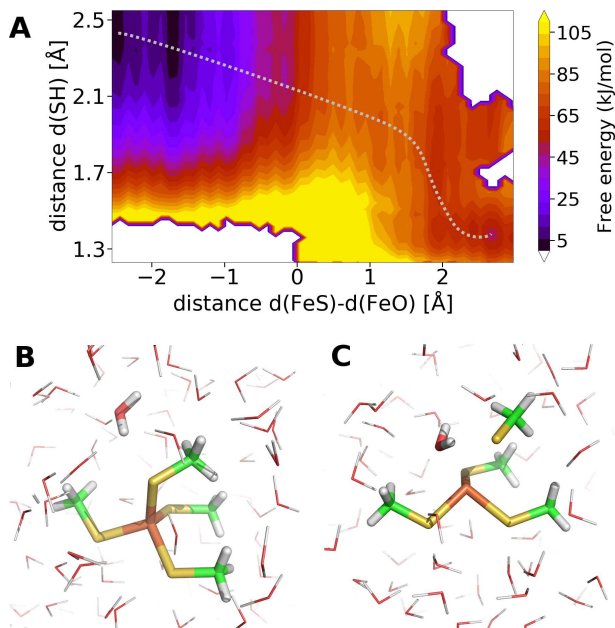
The two-dimensional free energy surface

Figure 2: Hydrolysis of $Fe(SCH_3)_4^-$ (reaction A in Fig. 1) in explicit solvent. (A) Two-dimensional free energy profile for the reaction in aqueous solution obtained with a hybrid QM/MM potential. Gray dashed line shows the approximate minimum free energy pathway. Snapshots of the (B) reactant and (C) transition states show the reactive atoms in sticks with Fe in orange, S in yellow, O in red and C in green.

in Fig. 2 shows that reaction A proceeds through a classical nucleophilic substitution mechanism (SN_2 or AnDn in the updated nomenclature) with a late TS, where the Fe–S bond is largely broken and the Fe–O bond is partially formed. The transferred proton is still fully bound to water and coordinated with the leaving group sulfur (at 1.98 Å distance, Table 2). A snapshot of the TS structure is shown in Fig 2C. In the reactant state, the reactive water hydrogen bonds to the leaving group sulfur (Fig 2B) and the surface topology is rather shallow because of water flexibility. But the surface rises up steeply for proton transfer if the Fe–S bond is not significantly broken, as expected from the basicity of the bound thiolate group in comparison to water (or its conjugate base, hydroxide). The TS region is rather flat [0.5<d(FeS)-d(FeO)<1.5 Å and 1.7<d(SH)<2.1 Å] with the minimum free energy pathway passing through a barrier of 82±5 kJ/mol (Table 2). On the other hand, the product basin

is deeper with a reaction free energy of 51±5 kJ/mol. Thus, reaction A is not spontaneous with slow activation kinetics (in relation to the thermal energy).

Table 2: Free energies (ΔG, in kJ/mol) and reaction coordinates (in Å) for stationary species of reaction A in explicit (QM/MM, as shown in Fig. 2) and implicit (M06+COSMO) solvents.

QM/MM	React	TS	Product
d(SH)[a]	2.40	1.98	1.39
d(FeS)-d(FeO)[a]	-2.43	1.28	2.75
ΔG	0.0	82±5	51±5
M06+COSMO			
d(SH)[b]	2.47	1.79	1.35
d(FeS)-d(FeO)[b]	-1.60	0.89	3.68
ΔG	0.0	85	43

[a] Mean values from state basins. Standard deviations are 0.04-0.05 Å for all states, except for d(FeS)-d(FeO) in the reactant state where the deviation is 0.16Å. [b]Geometries of ion-molecule complexes were used for reactant and product states.

Reaction A in implicit solvent also follows an AnDn mechanism with a late TS (Table 2). Proton reaction coordinates at stationary species are equivalent to those found in the explicit model. Differences in the iron reaction coordinate are due to water flexibility and shallow free energy surface observed above (Fig. 2A). Thus, similar reaction mechanisms are obtained in both solvent models when using the same electronic structure method (OLYP with split-valence basis). Geometrical differences are due to the underlying topology of the free energy surface and lack of solvent hydrogen bonding in the implicit model.

Free energies in implicit solvent usually include electronic, thermal and entropic effects from the reactive molecules and solvent contributions.[59] The M06/def2-TZVP level of theory gives high quality electronic energies for FeS reactions (Table 1), so it was used here with the COSMO implicit solvent model[30] that accounts for the electrostatic component of solvation free energies. Zero-point energies

and thermal (enthalpic and entropic) contributions from reactive centers may be calculated by harmonic oscillator and rigid rotor approximations. However, these contributions are relatively small (Table S2) and may be unreliable for entropic effects when low-frequency vibrational modes are present.[60] This is indeed the case for TS_A resulting in spurious entropies (Table S2). Thus, thermal and entropic effects were not included and relative free energies in our implicit water model contained only electronic and solvent contributions.

Table 2 shows that reaction and barrier free energies are within 8 kJ/mol (or 3 kJ/mol considering the statistical uncertainty of free energy simulations) between the two solvent models. This good agreement is partially fortuitous, due to error-cancelation and inclusion of different contributions. Nevertheless, we may conclude from these two sections of model calibration that geometries determined by OLYP functional with a split-valence basis set and energetics obtained with the M06/def2-TZVP level and implicit solvation are a reasonably reliable and efficient procedure to explore the reactivity of FeS clusters in aqueous solution.

3.3 Substitution and protonation reactions

Consecutive cleavage of two Fe–S bonds should be enough to disrupt mono- and polynuclear FeS clusters. Here, all feasible combinations of the 19 reactions shown in Fig. 1 that start with the ferric mononuclear FeS cluster model and lead to two Fe–S bond ruptures were considered. Reaction combinations were divided in groups without, with one and with two protonations of reactive species. These groups may correspond to reaction sequences in neutral, mildly acidic and highly acidic aqueous solutions, respectively.

Given the high barrier (see below) and the unlike event of thiolate dissociation at low pH, no combination involving a thiolate anion in acidic media (*e.g.*, C→D→J→N or F→K→Q) was examined. TS for protonation reactions were not considered as barriers for proton transfer were assumed to be smaller

than other reactions. This is certainly true for proton addition to anions, but may not hold for reactions J and P, where protonation and hydrolysis may proceed concerted. After applying the above criteria, there are 20 possible reaction combinations for which free energy profiles of reaction are shown in Fig. 3, 4 and 5.

In neutral aqueous solution (Fig. 3), nucleophilic substitution reactions (A and B) have high barriers (85 and 65 kJ/mol, respectively). These may be thermically activated and lead to products more stable than dissociative reactions (C, E and Q), which also have much higher barriers (200, 190 and 170 kJ/mol). Thus, the A→B reaction sequence will account for the rupture of up to two Fe–S bonds in FeS clusters and no thiolate dissociation will be observed in neutral solution.[11] This also suggests that spin-crossings previously identified in thiolate dissociation (Dn) reactions of stretched rubredoxin[15] should not contribute to the reactivity of FeS exposed to water. In both A and B reactions, a late TS is found with the proton transferred from the attacking water to the leaving group simultaneously to the reaction at the iron center. Details of this concerted reactions are given above for reaction A in explicit solvent.

Reaction profiles are significantly stabilized when one reactive species is protonated, such as in mildly acidic solution or when only part of a FeS cluster is exposed to acidic solution (Fig. 4). If protonation takes place after the first Fe–S bond rupture, the barrier for the second rupture via dissociative reaction L is 105 kJ/mol, lower than thiolate dissociation but still higher than the barrier for the substitution (AnDn) reaction H, 70 kJ/mol. P_H is also 75 kJ/mol more stable than P_L, thus the sequence A→G→H is kinetic and thermodynamically preferred. Similar to TS_A discussed above, TS_H is also late with the Fe–S bond largely broken and the Fe–O bond almost formed [d(FeS)-d(FeO)=1.2 Å]. The transferred proton is still bound to water and coordinates the sulfur in the leaving group [d(SH)=2.0 Å].

In acidic solution it is most likely that protonation will take place before bond rupture,
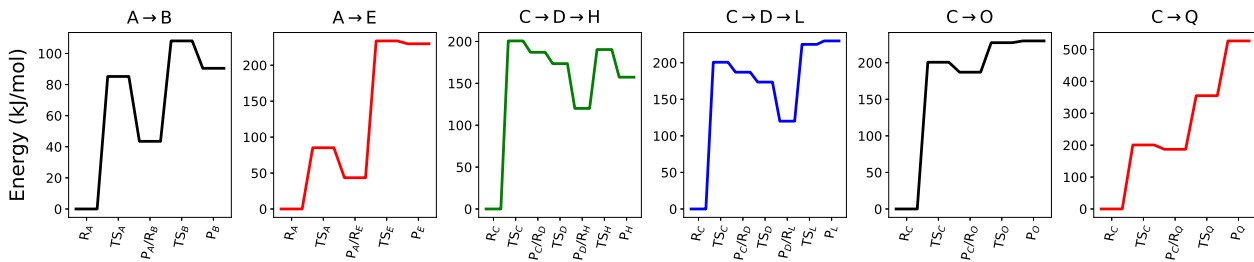
Figure 3: Reaction profiles for hydrolysis of oxidized mononuclear FeS cluster model in neutral aqueous solution. Reaction combinations are shown on top of each profile using the letter code given in Fig. 1. Reaction species are shown in the abscissa using R for reactant, TS for transition state and P for product, with the corresponding reaction subscripted.
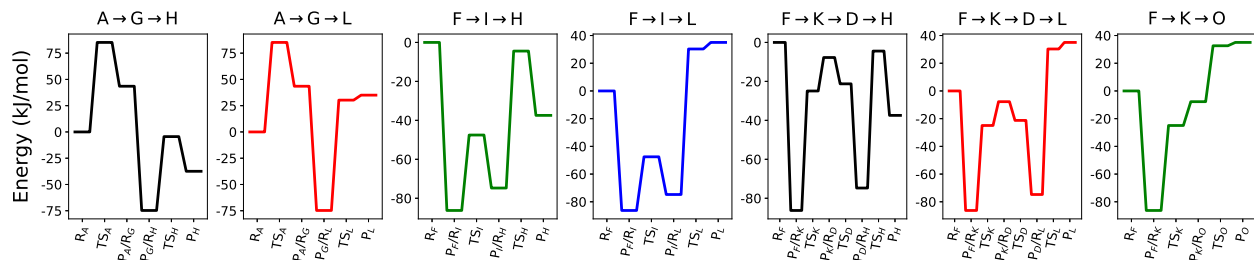

Figure 4: Reaction profiles for the hydrolysis of oxidized mononuclear FeS cluster model with one protonation, corresponding to mildly acidic solution.
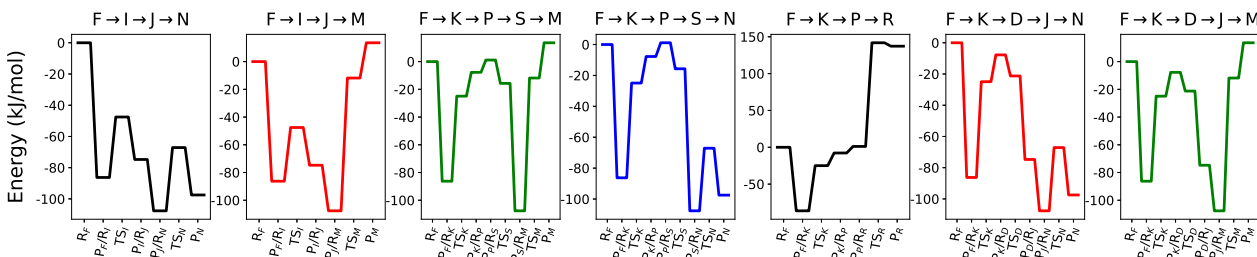

Figure 5: Reaction profiles for the hydrolysis of oxidized mononuclear FeS cluster model with two protonations, corresponding to highly acidic solution.

as soon as the FeS cluster is exposed to solvent. Protonation stabilizes the mononuclear FeS cluster by 85 kJ/mol but also eases the Fe–S bond rupture. Reactions I (AnDn) and K (Dn) may compete as their barriers are 40 and 60 kJ/mol, respectively. But P_I is much more stable than P_K. Protonation of the leaving group advances Fe–S rupture in TS_I resulting in an early TS [d(SH)=1.4 Å and d(FeS)-d(FeO)=0.2 Å]. The second Fe–S rupture follows the discussion of the previous paragraph, so the sequence F→I→H should be observed in mildly acidic solution. Other reaction combinations will give unstable products.

Bond cleavage in FeS clusters fully exposed to acidic solution or in highly acidic media

will proceed with both thiol leaving groups protonated (Fig. 5). The first Fe–S rupture should occur via reaction I, as in the previous paragraph. The second Fe–S rupture will proceed via the substitution (AnDn) reaction N with a barrier of 40 kJ/mol, whereas the dissociative reaction M has a high barrier, 100 kJ/mol. TS_N is again a late TS [d(SH)=1.4 Å and d(FeS)-d(FeO)=1.0 Å] but with dissociative character, as Fe–S and Fe–O bonds are almost not formed. Note that the first leaving group protonation will halve reaction barriers of substitution reactions (e.g., $TS_A \times TS_I$) or even cut to one-third those of dissociative reactions ($TS_C \times TS_K$). But a second protonation has no effect in the barrier of substitution reactions and actually increase the

8

barrier of dissociative reactions (M and R). We conclude the combination F→I→J→N is preferred in highly acidic solution. Sequences F→K→P→S→N and F→K→D→J→N will lead to the same products, but they have to climb higher barriers and hence will be slower.

4 Conclusions

To be written...

References

(1) Beinert, H. Iron-Sulfur Proteins: Ancient Structures, Still Full of Surprises. *J. Biol. Inorg. Chem.* **2000**, *5*, 2–15.

(2) Beinert, H.; Holm, R. H.; Munck, E. Iron-Sulfur Clusters: Nature's Modular, Multipurpose Structures. *Science* **1997**, *277*, 653–659.

(3) Noodleman, L.; Peng, C.; Case, D.; Mouesca, J.-M. Orbital Interactions, Electron Delocalization and Spin Coupling in Iron-Sulfur Clusters. *Coord. Chem. Rev.* **1995**, *144*, 199–244.

(4) Raugei, S.; Seefeldt, L. C.; Hoffman, B. M. Critical computational analysis illuminates the reductive-elimination mechanism that activates nitrogenase for N_2 reduction. *Proc. Natl. Acad. Sci. USA* **2018**, *115*, E10521–E10530.

(5) Sippel, D.; Rohde, M.; Netzer, J.; Trncik, C.; Gies, J.; Grunau, K.; Djurdjevic, I.; Decamps, L.; Andrade, S. L. A.; Einsle, O. A bound reaction intermediate sheds light on the mechanism of nitrogenase. *Science* **2018**, *359*, 1484–1489.

(6) Beinert, H.; Kennedy, M. C.; Stout, C. D. Aconitase as Iron-Sulfur Protein, Enzyme, and Iron-Regulatory Protein. *Chem. Rev.* **1996**, *96*, 2335–2373.

(7) Rao, P. V.; Holm, R. H. Synthetic analogues of the active sites of iron-sulfur proteins. *Chem. Rev.* **2004**, *104*, 527–559.

(8) Henderson, R. A. Proton transfer to synthetic FeS-based clusters. *Coord. Chem. Rev.* **2005**, *249*, 1841–1856.

(9) Zheng, P.; Li, H. Highly Covalent Ferric-Thiolate Bonds Exhibit Surprisingly Low Mechanical Stability. *J. Am. Chem. Soc.* **2011**, *133*, 6791–6798.

(10) Zheng, P.; Chou, C.-C.; Guo, Y.; Wang, Y.; Li, H. Single Molecule Force Spectroscopy Reveals the Molecular Mechanical Anisotropy of the FeS4 Metal Center in Rubredoxin. *J. Am. Chem. Soc.* **2013**, *135*, 17783–17792.

(11) Zheng, P.; Arantes, G. M.; Field, M. J.; Li, H. Force Induced Chemical Reactions on the Metal Center in a Single Metalloprotein Molecule. *Nature Comm.* **2015**, *6*, 7569.

(12) Nunes-Alves, A.; Arantes, G. M. Mechanical unfolding of macromolecules coupled to bond dissociation. *J. Chem. Theory Comput.* **2018**, *14*, 282–290.

(13) Cramer, C. J.; Truhlar, D. G. Density Functional Theory for Transition Metals and Transition Metal Chemistry. *Phys. Chem. Chem. Phys.* **2009**, *11*, 10757–10816.

(14) Schroder, D.; Shaik, S.; Schwarz, H. Two-State Reactivity as a New Concept in Organometallic Chemistry. *Acc. Chem. Res.* **2000**, *33*, 139–145.

(15) Arantes, G. M.; Bhattacharjee, A.; Field, M. J. Homolytic Cleavage of Fe–S Bonds in Rubredoxin Under Mechanical Stress. *Angew. Chem. Int. Ed.* **2013**, *52*, 8144–8146.

(16) Arantes, G. M.; Taylor, P. R. Approximate Multiconfigurational Treatment of Spin-Coupled Metal Complexes. *J. Chem. Theory Comput.* **2010**, *6*, 1981–1989.

(17) Sharma, S.; Sivalingam, K.; Neese, F.; Chan, G. K.-L. Low-energy spectrum of iron-sulfur clusters directly from many-particle quantum mechanics. *Nature Chem.* **2014**, *6*, 927–933.

(18) Reiher, M.; Wiebe, N.; Svore, K. M.; Wecker, D.; Troyer, M. Elucidating reaction mechanisms on quantum computers. *Proc. Natl. Acad. Sci. USA* **2017**, *114*, 7555–7560.

(19) Dauter, Z.; Sieker, L. C.; Wilson, K. S. Refinement of rubredoxin from *Desulfovibrio vulgaris* at 1.0 Å with and without restraints. *Acta Cryst. B* **1992**, *48*, 42–59.

(20) Guthrie., R. D.; Jencks, W. P. IU-PAC Recommendations for the Representation of Reaction Mechanisms. *Acc. Chem. Res.* **1989**, *22*, 343–349.

(21) Handy, N. C.; Cohen, A. J. Left-Right Correlation Energy. *Mol. Phys.* **2001**, *99*, 403–412.

(22) Lee, C.; Yang, W.; Parr, R. Development of the Colle-Salvetti Correlation-Energy Formula into a Functional of the Electron Density. *Phys. Rev. B* **1988**, *37*, 785–789.

(23) Ditchfield, R.; Hehre, W.; Pople, J. A. Self-Consistent Molecular-Orbital Methods. IX. An Extended Gaussian-Type Basis for Molecular-Orbital Studies of Organic Molecules. *J. Chem. Phys.* **1971**, *54*, 724–728.

(24) Tomasi, J.; Persico, M. Molecular Interactions in Solution: An Overview of Methods Based on Continuous Distributions of the Solvent. *Chem. Rev.* **1994**, *94*, 2027 – 2094.

(25) Frisch, M. J. et al. Gaussian 09, Revision A.1. Gaussian, Inc., Wallingford CT, 2009.

(26) Arantes, G. M.; Field, M. J. Ferric-Thiolate Bond Dissociation Studied with Electronic Structure Calculations. *J. Phys. Chem. A* **2015**, *119*, 10084–10090.

(27) Field, M. J. The pDynamo Program for Molecular Simulations using Hybrid Quantum Chemical and Molecular Mechanical Potentials. *J. Chem. Theory Comput.* **2008**, *4*, 1151–1161.

(28) Neese, F. *Wiley Interdisciplinary Reviews: Computational Molecular Science*; John Wiley & Sons, Ltd, 2012; Vol. 2; pp 73–78.

(29) Weigend, F.; Ahlrichs, R. Balanced Basis Sets of Split Valence, Triple Zeta Valence and Quadruple Zeta Valence Quality for H to Rn: Design and Assessment of Accuracy. *Phys. Chem. Chem. Phys.* **2005**, *7*, 3297–3305.

(30) Klamt, A. Conductor-like Screening Model for Real Solvents: A New Approach to the Quantitative Calculation of Solvation Phenomena. *J. Phys. Chem.* **1995**, *99*, 2224–2235.

(31) McQuarrie, D. A. *Statistical Mechanics*, 1st ed.; Harper and Row: New York, 1976.

(32) Hehre, W. J.; Radom, L.; Schleyer, P. R.; Pople, J. A. *Ab Initio Molecular Orbital Theory*, 1st ed.; Wiley: New York, 1986.

(33) Perdew, J. P.; Burke, K.; Ernzerhof, M. Generalized Gradient Approximation Made Simple. *Phys. Rev. Lett.* **1996**, *77*, 3865–3868.

(34) Becke, A. D. Density Functional Thermochemistry. III. The Role of Exact Exchange. *J. Chem. Phys.* **1993**, *98*, 5648.

(35) Tao, J. M.; Perdew, J. P.; Staroverov, V. N.; Scuseria, G. E. Climbing the Density Functional Ladder: Nonempirical Meta-Generalized Gradient Approximation Designed for Molecules and Solids. *Phys. Rev. Lett.* **2003**, *91*, 146401.

(36) Zhao, Y.; Truhlar, D. G. The M06 Suite of Density Functionals for Main Group Thermochemistry, Thermochemical Kinetics, Noncovalent Interactions, Excited States, and Transition Elements: Two New Functionals and Systematic Testing of Four M06-Class Functionals and 12 Other Functionals. *Theor. Chem. Acc.* **2008**, *120*, 215–241.

(37) Zhao, Y.; Truhlar, D. G. A new local density functional for main-group thermochemistry, transition metal bonding, thermochemical kinetics, and noncovalent interactions. *J. Chem. Phys.* **2006**, *125*, 194101.

(38) Mardirossiana, N.; Head-Gordon, M. ωB97X-V: A 10-parameter, range-separated hybrid, generalized gradient approximation density functional with nonlocal correlation, designed by a survival-of-the-fittest strategy. *Phys. Chem. Chem. Phys.* **2014**, *16*, 9904–9924.

(39) Weigend, F. Accurate Coulomb-Fitting Basis Sets for H to Rn. *Phys. Chem. Chem. Phys.* **2006**, *8*, 1057–1065.

(40) Grimme, S.; Antony, J.; Ehrlich, S.; Krieg, H. A consistent and accurate ab initio parametrization of density functional dispersion correction (DFT-D) for the 94 elements H-Pu. *J. Chem. Phys.* **2010**, *132*, 154104.

(41) Becke, A. D.; Johnson, E. R. A density-functional model of the dispersion interaction. *J. Chem. Phys.* **2005**, *123*, 154101.

(42) Johnson, E. R.; Becke, A. D. A post-Hartree-Fock model of intermolecular interactions. *J. Chem. Phys.* **2005**, *123*, 024101.

(43) Stewart, J. J. P. Optimization of Parameters for Semiempirical Methods V: Modification of NDDO Approximations and Application to 70 Elements. *J. Mol. Model.* **2007**, *13*, 1173–1213.

(44) Helgaker, T.; Jørgensen, P.; Olsen, J. *Molecular Electronic-Structure Theory*, 1st ed.; Wiley: New York, 2000.

(45) Granucci, G.; Toniolo, A. Molecular Gradients for Semiempirical CI Wavefunctions with Floating Occupation Molecular Orbitals. *Chem. Phys. Lett.* **2000**, *325*, 79–85.

(46) Slavícek, P.; Martínez, T. J. Ab Initio Floating Occupation Molecular Orbital-Complete Active Space Configuration Interaction: An Efficient Approximation to CASSCF. *J. Chem. Phys.* **2010**, *132*, 234102.

(47) Riplinger, C.; Pinski, P.; Becker, U.; Valeev, E. F.; Neese, F. Sparse maps-A systematic infrastructure for reduced-scaling electronic structure methods. II. Linear scaling domain based pair natural orbital coupled cluster theory. *J. Chem. Phys.* **2016**, *144*, 024109.

(48) Neese, F. Software update: the ORCA program system, version 4.0. *Wiley Interdiscip. Rev. Comput. Mol. Sci.* **2018**, *8*, e1327.

(49) Huang, J.; MacKerell Jr, A. D. CHARMM36 all-atom additive protein force field: Validation based on comparison to NMR data. *J. Comp. Chem.* **2013**, *34*, 2135–2145.

(50) Jorgensen, W. L.; Chandrasekhar, J.; Madura, J. D.; Impey, R. W.; Klein, M. L. Comparison of simple potential functions for simulating liquid water. *J. Chem. Phys.* **1983**, *79*, 926–935.

(51) Arantes, G. M.; Ribeiro, M. C. C. A microscopic view of substitution reactions solvated by ionic liquids. *J. Chem. Phys.* **2008**, *128*, 114503.

(52) Arantes, G. M. The catalytic acid in the dephosphorylation of the Cdk2-pTpY/CycA protein complex by Cdc25B phosphatase. *J. Phys. Chem. B* **2008**, *112*, 15244–15247.

(53) Torrie, G. M.; Valleau, J. P. Nonphysical Sampling Distributions in Monte Carlo Free-Energy Estimation: Umbrella Sampling. *J. Comp. Phys.* **1977**, *23*, 187–199.

(54) Allen, M.; Tildesley, D. *Computer Simulation of Liquids*, 1st ed.; Oxford University Press: New York, 1987.

(55) Roux, B. The calculation of the potential of mean force using computer simulations. *Comp. Phys. Comm.* **1995**, *91*, 275–282.

(56) Johnson, R. W. An introduction to the bootstrap. *Teaching Statistics* **2001**, *23*, 49–54.

(57) Buhl, M.; Kabrede, H. Geometries of Transition-Metal Complexes from Density-Functional Theory. *J. Chem. Theory Comput.* **2006**, *2*, 1282–1290.

(58) Field, M. J.; Bash, P. A.; Karplus, M. A combined quantum mechanical and molecular mechanical poteintial for molecular dynamics simulations. *J. Comput. Chem.* **1990**, *11*, 700–733.

(59) Chien, T. C.; Dias, L.; Arantes, G.; Santos, L.; Triboni, E.; Bastos, E. L.; Politi, M. J. 1-(2-Quinolyl)-2-naphthol: A new intra-intermolecular photoacid-photobase molecule. *J. Photochem. Photobiology A* **2008**, *194*, 37–48.

(60) Ayala, P.; Schlegel, H. B. Identification and treatment of internal rotation in normal mode vibrational analysis. *J. Chem. Phys.* **1998**, *108*, 2314–2325.

Supporting Information

Modelling the hydrolysis of iron-sulfur clusters

Murilo H. Teixeira, Felipe Curtolo, Sofia R. G. Camilo, Martin J. Field, Peng Zheng, Hongbin Li and Guilherme M. Arantes

Table S1: Serial computational timings (in minutes) for a complete energy calculation of the isolated $Fe(SCH_3)_4^-$ molecule with the def2-TZVP basis (except M06L/SVP and OLYP/SVP) and the ORCA program running in an Intel E5-2670 CPU.

Method	Time
B3LYP-D3	24
CCSD(T)	165
M06	24
M06L	2
M06L/SVP	0.7
OLYP	2
OLYP/SVP	0.5
ωB97X-D3	52

Table S2: Zero-point energy (ZPE), enthalpic (H) and entropic (S) contributions at 300 K for stationary species along the water substitution of $Fe(SCH_3)_4^-$ (reaction A in Fig. 1) in implicit solvent. Absolute values in *Hartree* are shown for the reactant state. For TS and product state, relative values to the reactant are shown in kJ/mol. $S_{<900k}$ was obtained removing contributions from vibrational temperatures <900 K.

	Reactant	TS	Product
ZPE	0.172002	3.1	-3.8
H	0.193168	-6.3	-7.3
S	0.092555	-67.1	5.0
$S_{<900K}$	0.058681	-52.4	19.4